THE JOURNAL OF PHYSICAL CHEMISTRY Letters

Perspective

pubs.acs.org/JPCL

Polarization-Controlled Raman Microscopy and Nanoscopy

Yuika Saito* and Prabhat Verma

Department of Applied Physics, Osaka University, 2-1 Yamadaoka, Suita, Osaka, 565-0871 Japan

ABSTRACT: Polarization imaging reveals unique characteristics of samples, such as molecular symmetry, orientation, or intermolecular interactions. Polarization techniques extend the ability of conventional spectroscopy to enable the characterization and identification of molecular species. In the early days of spectroscopy, it was considered that a set of polarizers placed in the illumination and the detection paths was enough to enable polarization analysis. However, with the development of new microscope imaging techniques, such as high-resolution microscopy, nonlinear spectroscopic imaging, and near-field microscopy, the inevitable polarization changes caused by external optical components needs to be discussed. In this Perspective, we present some of the hot topics that are specific to high-spatial-resolution microscopy and introduce recent related work in the field. Among the many spectroscopic techniques available, we focus in particular on Raman spectroscopy because Raman tensors are widely used in pure and applied sciences to study the symmetry of matter.

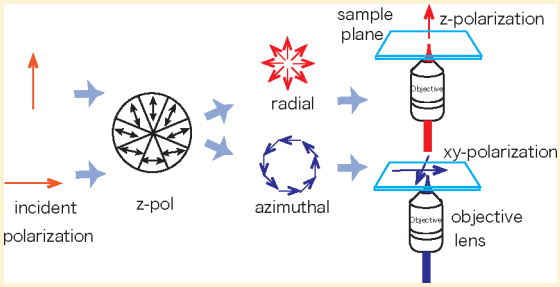

Microscopy and nanoscience have seen rapid advances, and polarization analysis in high-spatial-resolution imaging is one issue that has recently been a topic of discussion. When a light beam travels in a collimated path, the polarization is easily analyzed by inserting a polarizer into the light path; however, when it is tightly focused, the polarization distribution inside of the focal area is not homogeneous because of interference effects caused by local electric fields propagating in different directions. At the same time, the polarization of scattered light exhibits an angular dependence, which means that measurements cannot be performed in a straightforward way. In this Perspective, we will review recent techniques for measuring polarization in tightly focused light, together with some new aspects of polarization control that are important for spectroscopic imaging.

Polarization Raman Spectroscopy. Among the many available spectroscopic techniques, polarization measurement in linear or nonlinear Raman spectroscopy has been studied for many years, in accordance with the development of the theory of Raman tensors.[1] Light polarization is determined by the orientation of electric field oscillations in the plane perpendicular to the propagation direction, and symmetry analysis through the molecular vibrations is a standard application of polarization spectroscopy. In addition, under resonance excitation conditions, polarization Raman spectroscopy can probe even the electronic states of molecules through vibronic coupling.[2] Besides the ability to investigate the properties of single molecules, polarization measurements are useful for their application in the collective state of samples. Especially for crystals, polarization Raman measurements have been widely used to characterize local strain and defects, which are directly linked to the characteristic Raman peaks.[3−5] Orientational analysis has been extended to other samples, such as liquid crystals,[6] polymers,[7] and molecular thin films,[8] and has the potential to be applied to complex biological samples too. Polarization spectroscopy has often been combined with not only Raman spectroscopy but also fluorescence spectroscopy and second harmonic generation microscopy.[9]

Polarization Raman Microscopy. Here, we would consider polarization Raman spectroscopy in a microscopic setup. By employing a high-numerical-aperture (NA) microscope objective lens, it is possible to realize a spatial resolution close to the diffraction limit, which is about half of the incident light wavelength. In conventional polarization microscopy, only two polarization components are available, the *x*- and *y*-polarizations (parallel to the sample plane). The *z*-polarization (perpendicular to the sample plane) is not available even though the sample distribution is not restricted to two dimensions. When it is necessary to study the sample under *z*-polarization excitation, we have to rotate the sample in the direction parallel to the molecular axis, which is not always possible in microscopic conditions where the working distance of the objective lens limits the available space. Turrell suggested in 1984 that, with a high-NA objective lens, the *z*-polarization ratio is not negligible compared with the *x*- and *y*-polarizations.[10] For example, in an oil-immersion objective (NA = 1.4), the *z*-polarization ratio becomes more than 20% of the total incident field even if perfect linear polarization is introduced.[11] This property holds promise for creating *z*-polarization components under a microscope. The key requirements for achieving control over *z*-polarization in microscopes are a high-NA objective lens and modulation of the incident polarization pattern by using a spatial light modulator (SLM). In the following, we

Received: February 22, 2012
Accepted: April 26, 2012
Published: April 26, 2012

 © 2012 American Chemical Society dx.doi.org/10.1021/jz300213t | *J. Phys. Chem. Lett.* 2012, 3, 1295−1300

describe three-dimensional polarization measurements enabled by using a kind of SLM called *z*-pol.

Figure 1 schematically illustrates the formation of *x*, *y*, and *z* polarizations by utilizing the *z*-pol. Of the two incident light

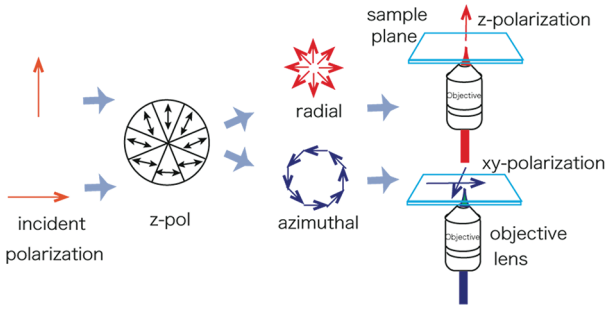

Figure 1. Schematic illustration of polarization control using a *z*-pol device, an eight-segment half-wave plate in which the polarization direction in each segment is tilted by 22.5° relative to the neighboring segments. First, radial or azimuthal polarizations are formed, and these are then introduced to a high-NA objective lens and tightly focused on the sample plane to form either *xy*-polarization (parallel) or *z*-polarization (perpendicular to the sample plane).

polarizations, radial and azimuthal, when they are focused on a sample plane, only the radial polarization is responsible for creating the *z*-polarization. Therefore, if the incident light consists of only the radial polarization, a highly *z*-polarization-dominant field is formed at the sample plane. By employing a *z*-pol, which is an eight-segment half-wave plate in which each segment has a different polarization angle, we can realize a quasi-radial polarization. The polarization at the sample in this configuration can be switched between *xy*- or *z*-directions by rotating the incident polarization. An annular mask is inserted in the incident laser path to exclude small-NA (<1) components in order to achieve highly *z*-polarization-dominant excitation. The high-NA objective lens effectively modifies the angle of incidence with respect to the sample plane to make the radial polarization perpendicular to the sample surface. The analyzer was set in the direction that corresponds to the crossed Nichols setting to the incident linear polarization.

Here, we present an example of *z*-polarization measurement using alpha-quartz. Of the 27 normal modes in alpha-quartz, we pay particular attention to two modes with different symmetries, the A_1 (464 cm^{-1}) and E modes (394 cm^{-1}). The incident *z*-polarization can excite only the A_1 mode and not the E mode, as expected from the Raman tensor.[12] The expected Raman signal intensity of each vibrational mode is determined by multiplying three factors, the incident light intensity, the corresponding Raman tensor, and the detection efficiency. The signal collection efficiencies for the *xy*-direction and the *z*-direction in the backscattering configuration are given by factors *A* and *B*, respectively, which are shown below as a function of the objective lens cone angle θ_m[10]

$$A = \pi^2\left(\frac{4}{3} - \cos\theta_w - \frac{1}{3}\cos^3\theta_w\right) \quad (1)$$

$$B = \pi\left(\frac{2}{3} - \cos\theta_w + \frac{1}{3}\cos^3\theta_w\right) \quad (2)$$

It turns out from eqs 1 and 2 that *B* is about 10% of *A*, even in the case of NA = 1.4, suggesting that for linearly polarized incident light, the *zz* tensor components are barely detectable, even with a high-NA objective lens. Therefore, in order to observe the *z*-polarization component, it would be necessary to modify the incident laser polarization.

Figure 2 shows polarization measurements of the Raman spectra from alpha-quartz obtained with NAs of (a) 0.15,

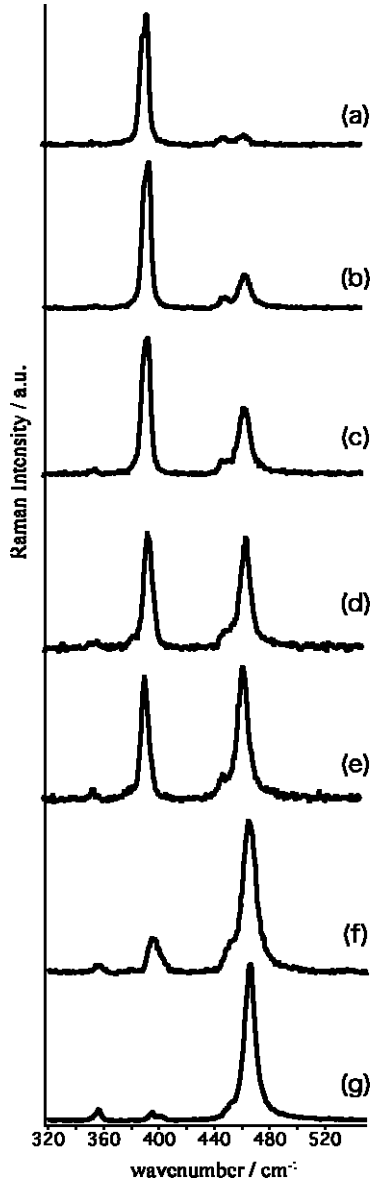

Figure 2. Micro-Raman spectra of alpha-quartz obtained with objective lenses having different NAs, (a) 0.15, (b) 0.3, (c) 0.45, (d) 0.8, (e) 0.9, (f) 1.4, with an annular mask, and (g) 1.4, with an annular mask and *z*-pol. With the combination of the *z*-pol, the *z*-polarization sensitive Raman mode at 464 cm^{-1} becomes dominant, whereas the mode at 394 cm^{-1} becomes suppressed.

(b) 0.3, (c) 0.45, (d) 0.8, and (e) 0.9. The A_1 mode at 464 cm^{-1} gradually become stronger with an increasing value of NA, showing that stronger *z*-polarization is created by a higher value of NA. (f) is the spectrum obtained for NA = 1.4 with an annular mask, and (g) is the spectrum obtained for NA = 1.4 with an annular mask and the *z*-pol. In (f), the *z*-polarization at 464 cm^{-1} was successfully intensified with respect to the other modes by virtue of the annular mask excluding low-NA components.

dx.doi.org/10.1021/jz300213t | *J. Phys. Chem. Lett.* 2012, 3, 1295−1300

In (g), with the *z*-pol, we can see that the *z*-polarization component at 464 cm^{-1} is dominant to the extent that it almost overwhelms the other modes. Compared with the spectrum in (f), it is obvious that the spectrum in (g) has a much stronger dominance of the *z*-polarization.

Realizing the designed configurations requires a variety of SLMs.

Development of a New SLM. As the experimental results obtained with the *z*-pol suggest, the key feature of our new polarization microscopy is deeply concerned with the idea of designing the illumination configuration. The idea of structured illumination has a long history,[13−17] though not many of them are aimed at polarization analysis. Realizing the designed configurations requires a variety of SLMs. One example is a tunable waveplate formed of a liquid crystal layer that is driven by an external voltage to rapidly modulate the polarization during measurement. There are SLMs that consist of hundreds of pixels, each controlled separately either in amplitude or in phase. SLMs are mainly designed for pulse shaping, multipoint illumination, optical fabrication, optical compensation, and so forth, rather than polarization measurement, and there is a rapidly growing number of commercially available SLMs with increasing flexibilities.[18] A novel photofabrication method for making a SLM has been reported.[19] By exploiting the ability of femtosecond lasers to create subwavelength anisotropic modifications inside of silica glass, a polarization vortex converter, operating in the visible region, has been demonstrated. A significant advantage of the technique is the possibility of achieving radial or azimuthal polarization with a single optical element simply by controlling the handedness of the incident circular polarization. Another example is preferential molecular alignment achieved in pentacene films by using photoaligned azo-polyimide films as the substrate.[20] The photoalignment method is a promising technique for achieving spatially variable alignment. The ultimate SLM would be the one that is made by manipulating the orientation of each molecule on a thin film device to form a desirable pattern. With the recent remarkable developments made in SLM technology, this may not be just a dream in the near future.

Polarization Raman Nanoscopy. The resolving powers of optical microscopes are limited by the wave nature of light. For example, an optical microscope can acquire images with a resolution of about 300 nm with an excitation wavelength of 500 nm when equipped with an objective lens with NA = 1. While there have been attempts to overcome this diffraction limit by using nonlinear spectroscopy, near-field optics has emerged as an indispensable tool for subwavelength imaging and could provide better detection accuracy. Unlike other optical microscopes, the concept of the near-field microscope is based on the spatial confinement of incident light interacting with nanostructures to a value much smaller compared to the wavelength of the incident light.[21] The spatial resolution is determined by the size of the probe apex, which can ultimately be as small as a few molecules. With the aid of a scanning tunneling microscope (STM) and atomic force microscope (AFM), near-field microscope techniques have matured. Signal enhancement is very useful in near-field microscopy with a reduced sample volume, especially for Raman spectroscopy, which shows much smaller cross sections, typically only 10^{-10} or lower, compared with fluorescence or IR absorption spectroscopy. Raman scattering from molecules in close proximity to the metallic nanostructures is strongly enhanced due to the excitation of localized surface plasmon polaritons. This phenomenon is known as surface-enhanced Raman scattering (SERS), the enhancement factor[22] of which has been reported to reach 10^5−10^{20} . The inclusion of a metallic probe tip in a system based on SERS yields encouraging results as the probe can act as a nanometric light source. Work on tip-enhanced Raman spectroscopy (TERS) has been reported by many researchers since the first report in 2000.[23,24]

Because the spatial resolution of TERS is ∼20 nm, the polarization distribution within a comparatively large focal area needs to be considered. When linearly polarized light is tightly focused by a high-NA objective lens, the polarization at the focal plane consists of both *xy*-components and *z*-components. Besides this polarization admixture, the field intensity distributions of each component cause a problem when the spatial resolution reaches the nanometer scale.[25] Figure 3 shows the calculated field intensity distribution in the focal plane for linearly polarized (*x*-direction) light tightly focused by an objective lens (NA = 1.4), showing (a) the *z*-polarization and (b) the *xy*-polarization. The electric field of the *z*-polarization is canceled at the center of the spot, creating two side peaks, as shown in Figure 3a. On the other hand, the field intensity of the *xy*-polarization shows a maximum at the center, as seen in Figure 3b. On the other hand, radially or azimuthally distributed polarizations create highly pure *z*- or *xy*-polarizations. Figure 3c and d shows the calculated total electric field intensity distributions at a tightly focused spot using radial (*z*-) and azimuthal (*xy*-) polarizations. In the *z*-polarization configuration, the electric field intensity in the longitudinal direction (along the tip axis) is the strongest at the center, as shown in Figure 3c. In the *xy*-polarization configuration, the lateral field intensity is the strongest at the circumference, as in Figure 3d. Note that areas dominated by both the *x*-polarization and *y*-polarization are formed in the case of this configuration. According to these predictions, the polarization components are spatially distributed in quite different ways.

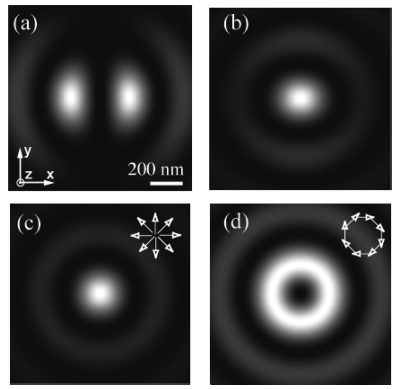

Figure 3. Incident light intensity distributions in the focal point: (a) *z*-polarization component with linear incident polarization, (b) *xy*-polarization component with linear incident polarization, (c) *z*-polarization component with radially patterned incident polarization, and (d) *xy*-polarization component with azimuthally patterned incident polarization. Objective lens NA = 1. 4; incident light wavelength = 500 nm.

We earlier introduced polarization analysis in a TERS experiments.[26] In near-field spectroscopy, the polarization direction is

dx.doi.org/10.1021/jz300213t | *J. Phys. Chem. Lett.* 2012, 3, 1295−1300

characterized by two components of the electric field polarization on the sample, the *xy*-polarization (perpendicular to the tip axis) and the *z*-polarization (parallel to the tip axis). As we showed in that study, one needs to adjust the tip to a certain position in the focal area to select either the *z*- or *xy*-polarization field components, which is possible in the TERS setup. Single-walled carbon nanotubes (SWNTs), which have strong polarization dependence, were investigated with this polarization control. The radial breathing mode (RBM) and the G-band, which belong to different vibrational symmetries, showed opposite polarization dependences. Figure 4 shows a

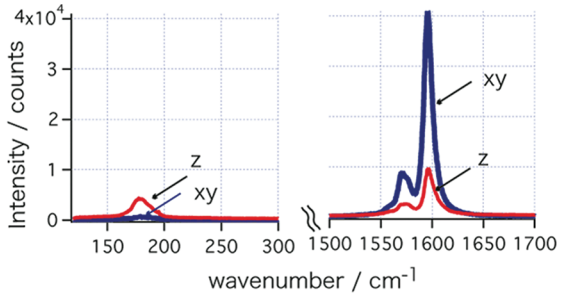

Figure 4. Near-field polarization Raman spectra of a SWNT obtained under *z*- or *xy*-polarization conditions. Under *z*-polarization (red line), RBM is well-enhanced, and under *xy*-polarization (blue line), the G-band is excited more efficiently compared with *z*-polarization.

comparison of the near-field Raman signal intensities of the SWNTs measured under *z*- and *xy*-polarization conditions. The near-field spectra were obtained by subtracting the spectra obtained without a tip from those obtained with a silver tip in contact with the sample. Red lines indicate the spectra measured under the *z*-polarization condition, and blue lines indicate those measured under the *xy*-polarization condition. Under the *z*-polarization condition, the RBM showed stronger enhancement in comparison to the G-band, which exhibited less enhancement. In contrast, under the *xy*-polarization condition, the G-band exhibited higher enhancement, whereas the RBM did not. That is, the RBM and G-band exhibited opposite enhancement behaviors between the two polarization conditions.

This figure indicates the selective enhancement of a particular vibrational mode by the near-field tip, which can be explained as follows. The explanation is based on the assumption that the tip apex, coated with silver particles, is excited by the incident laser field and acts as a single dipole, which in turn provides sufficient field enhancement in either the *z*- or *xy*-polarization according to the incident polarization configuration. Under each polarization, the tip-enhanced field has either a longitudinal or a lateral polarization, which couples with different electric resonances of the nanotubes. Vibrational transitions of the carbon nanotubes at this excitation wavelength couple with electron transitions either parallel or perpendicular to the tube axis.[27] Because the G-band contains a vibrational transition moment along the tube axis, it is effectively excited by *xy*-polarization. On the other hand, the vibrational transition moment of the RBM is located radially around the tube diameter and is more efficiently excited by the *z*-polarization than by the *xy*-polarization because the entire excitation field in the *z*-polarization is perpendicular to the tube axis.

Polarization Control by Nanostructures. In TERS microscopy, where the incident light is polarized parallel to the probe axis, the *z*-polarization is thought to be advantageous over the *xy*-polarization. While this is true for most samples under common near-field experimental conditions, there are samples that respond better to the *xy*-polarization due to their orientations. Indeed, there have been several reports that have discussed such samples. This leads us to an important requirement that the near-field experimental setup should be equipped with proper sensitivity for measurements with the *xy*-polarization. This requires not only creation of effective *xy*-polarized illumination at the near-field probe but also proper enhancement of *xy*-polarized light by the probe. In ref 28, the authors examined the *xy*-polarization enhancement sensitivity of near-field probes by measuring and evaluating the near-field Rayleigh scattering images constructed by a variety of probes and found that the *xy*-polarization enhancement sensitivity strongly depends on the sharpness of the apex of the near-field probes. A supporting FDTD simulation, as well as experimental results, showed that probes with larger apex diameters yield stronger scattering when illuminated with *xy*-polarized light. However, the experimental results also indicated that the contrast could not be improved only by increasing the diameter of the apex. They concluded that a metal coating thicker than 30 nm is necessary for *xy*-polarization sensitivity in a standard TERS system. To improve the *xy*-polarization sensitivity in TERS measurements further, there could still be some scope for optimizing the probe design, including the possibility of estimating the performance through calculations and simulations.[29,30] Not only the *xy*-polarization but also the depolarization effect should be considered as one of the important functions of the near-field probe.[31] The scattered Rayleigh signal from the near-field probe also plays a crucial role for the characterization of the stress tensor, determination of crystalline samples,[32] the molecular orientation[33], and nanocrystallography.[34]

Nanofabrication will be indispensable for future polarization nanoscopy because it may allow the incident polarization at the apex of a near-field probe to be controlled.

Nanofabrication will be indispensable for future polarization nanoscopy because it may allow the incident polarization at the apex of a near-field probe to be controlled. The light polarization is usually controlled by external optics, such as a polarizer or SLM; however, it would be preferable if the laser emission itself had the desired polarization pattern to avoid the power loss and deformation that are inevitable when using optical components. A promising result was recently presented by a group of scientists in Japan.[35] They fabricated a periodic nanoscale counterclockwise equilateral cross on a semiconductor film containing quantum dots by electron beam lithography. The emission polarization from the quantum dots showed different degrees of right and left circularity influenced by the chirality of the fabricated nanostructures. It has been generally accepted that we cannot modify the physical properties of matter just by changing its structure; however, through recent developments in nanotechnology and nanofabrication, such an idea has come to be seen as possible. Their results will lead to an important consequence that we can control the emission polarization in combination with nanostructures. The idea of nanofabrication for polarization control

will inevitably be applied to near-field probe design and many other aspects of polarization optics.

Polarization Nonlinear Raman Imaging. Spectroscopy basically involves the dimension of energy, whereas polarization is a vectorial quantity. This leads to an important application of polarization spectroscopy, namely, the ability to distinguish two species that appear otherwise identical in the energy dimension. Figure 5 shows Raman spectra of alpha-quartz obtained under

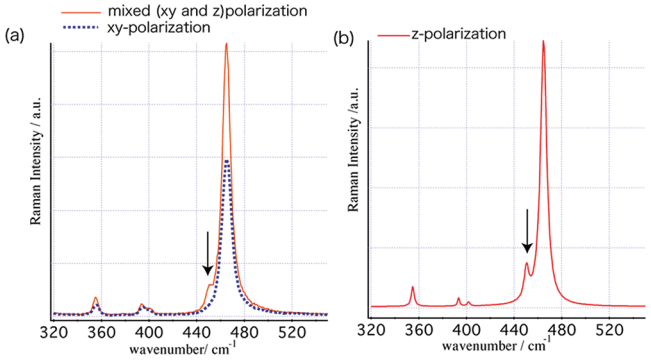

Figure 5. Polarization Raman spectra of alpha-quartz. (a) The orange line indicates the results obtained under mixed (*xy*- and *z*-) polarization excitation, and the dotted blue line indicates the result obtained under in-plane (*xy*-) polarization. The peak shown by the arrow appeared as a shoulder. (b) The *z*-polarization Raman spectra of alpha-quartz (red line). The data were constructed by subtracting the dotted blue line from the orange line in (a). The peak indicated by the arrow appeared clearly in (b) because of the polarization control.

different polarization conditions. The peak indicated by the arrow in Figure 5a appears only on a shoulder of the strong Raman peak nearby, whereas in Figure 5b, the peak is clearly separated due to the polarization control, enhancing the intensity ratio of the overlapped bands, which have different Raman tensor patterns. Figure 5 suggests that, even if the two species have the same vibrational energy, they can be separated on the polarization axis. This idea is conveniently used in nonlinear spectroscopy, that is, coherent antistokes raman scattering (CARS), for eliminating a nonresonant background to enhance the contrast.[36]

The interesting feature in polarization nonlinear Raman spectroscopy is that we can manipulate laser beams of two or more colors while controlling their polarizations separately.

For imaging with higher spatial resolution, nonlinear spectroscopy is a common approach. Since the development of stable high-power pulsed lasers and white-light continuum sources, the applications of nonlinear spectroscopy imaging, especially CARS and stimulated Raman spectroscopy (SRS) imaging, are now rapidly growing.[37,38] The interesting feature in polarization nonlinear Raman spectroscopy is that we can manipulate laser beams of two or more colors while controlling their polarizations separately. For example, in the case of polarization CARS, a resonant Raman signal was produced with a polarization direction θ that satisfied the equation $\tan\theta = \rho_R \tan\phi$,[36] where ϕ is the polarization angle between the pump beam and the Stokes beam and ρ_R is the depolarization ratio of the resonant third-order nonlinear polarization. Because the depolarization ratio of the nonresonant background, ρ_{NP}, is 1/3, it is possible to eliminate the nonresonant background through the Kleinman's symmetry by an analyzer directed toward the polarization perpendicular to the background. This is not the only way of achieving polarization control in CARS. Some groups have proposed an interferometric polarization CARS that effectively suppresses the nonresonant background while significantly amplifying the Raman signal for sensitive vibrational imaging with high contrast. By introducing a second Stokes beam with a polarization perpendicular to the first one and modulating the phase difference between the two interference CARS signals (IP-CARS), the technique yields a 6-fold improvement in the signal-to-background ratio.[39] Another group demonstrated that heterodyne interferometric polarization-CARS (HI-CARS) is an effective technique to simultaneously extract and amplify the resonant component of a CARS spectrum. In this method, the CARS field is combined at the detector with a local oscillator giving a phase offset between the two fields, allowing amplification of the weak CARS beam via interference with a much stronger local oscillator.[40] In polarization-controlled SRS, molecular vibrational motion temporally modulates the birefringence of the sample and thus produces oscillatory signals in Kerr measurements.[41] The polarization method is called Raman-induced Kerr-effect spectroscopy (RIKES) and can be considered a promising candidate for future polarization spectroscopy. Polarization measurement in nonlinear Raman spectroscopy is ideally suited for turnkey nonlinear Raman systems for spectroscopy and microscopy, including time-resolved measurements, because it requires minimal realignment and is capable of addressing vibrational structures in the fingerprint region without any interference of the nonresonant background.

AUTHOR INFORMATION

Corresponding Author

*E-mail: yuika@ap.eng.osaka-u.ac.jp.

Notes

The authors declare no competing financial interest.

Biographies

Yuika Saito obtained a Ph.D. from the Univeristy of Tokyo. After a postdoctoral stay at the University of Leeds in U.K., she joined Prof. Satoshi Kawata's laboratory at the Institute of Physical and Chemical Research (RIKEN). Since 2011, she has been an associate professor at Osaka University. Her current research interest focuses on the use of polarization in near-field microscopy.

Prabhat Verma (http://www.pverma.com/) obtained his Ph.D. in 1994 from the Indian Institute of Technology, Delhi, India. After postdoctoral stays at the TU Bergakademie, Freiberg in Germany, and Kyoto Institute of Technology in Japan, he joined Osaka University as Associate Professor. Since 2010, he has been a Professor in the Department of Applied Physics at Osaka University. His current research interests focus on nanospectroscopy, high-resolution near-field microscopy, plasmonics, and related fields.

REFERENCES

(1) *Raman Spectroscopy Theory and Practice*; Szymanski, H. A., Ed.; Plenum Press: New York, 1967.

(2) Hamaguchi, H.; Harada, I.; Shimanouchi, T. Anomalous Polarization in Resonance Raman Effect of Octahedral HexaChloridate (IV) Ion. *Chem. Phys. Lett.* **1975**, *32*, 103−107.
(3) Ossikovski, R.; Nguyen, Q; Picardi, G.; Schreiber, J. Determining the Stress Tensor in Strained Semiconductor Structures by using Polarized Micro-Raman Spectroscopy in Oblique Backscattering Configuration. *J. Appl. Phys.* **2008**, *103*, 093525.
(4) Liao, M. M. H. Local Stress Determination in Shallow Trench Insulator Structures with One-Side and Two-Sides Pad-SiN Layer by Polarized Micro-Raman Spectroscopy Extraction and Mechanical Modelization. *J. Appl. Phys.* **2009**, *105*, 093511.
(5) Gouadec, G.; Makaoui, K.; Perriere, L.; Colomban, P.; Mazerolles, L. Polarized Micro-Raman Study of Al_2O_3-Based Directionally Solidified Oxide Eutectics Containing $GdAlO_3$ Perovskite $Er_3Al_5O_{12}$ Garnet and Cubic ZrO_2. *J. Raman Spectrosc.* **2010**, *41*, 969−977.
(6) Castriota, M.; Fasanella, A.; Cazzanelli, E.; De Sio, L.; Caputo, R.; Umeton, C. In Situ Polarized Micro-Raman Investigation of Periodic Structures Realized in Liquid-Crystalline Composite Materials. *Opt. Express* **2011**, *19*, 10494−10500.
(7) Sourisseau, C. Polarization Measurements in Macro- and Micro-Raman Spectroscopies: Molecular Orientations in Thin Films and Azo-Dye Containing Polymer Systems. *Chem. Rev.* **2004**, *104*, 3851−3891.
(8) Muraki, N.; Yoshikawa, M. Polarized Micro-Raman Measurements of Cross Sections of Single- and Multi-Layer Organic Films on Glass Substrate. *Chem. Phys. Lett.* **2009**, *481*, 103−106.
(9) Brasselet, S. Polarization-Resolved Nonlinear Microscopy: Application to Structural Molecular and Biological Imaging. *Adv. Optics* **2011**, *3*, 205−271.
(10) Turrell, G. Analysis of Polarization Measurements in Raman Spectroscopy. *J. Raman Spectrosc.* **1984**, *15*, 103−108.
(11) Saito, Y.; Kobayashi, M.; Hiraga, D.; Fujita, K.; Kawano, S.; Inouye, Y.; Kawata, S. Z-Polarization Sensitive Detection in Micro-Raman Spectroscopy by Radially Polarized Incident Light. *J. Raman Spectrosc.* **2008**, *105*, 1643−1648.
(12) Masso, J. D.; She, C. Y.; Edwards, D. F. Effect of Inherent Electric and Anisotropic Forces on Raman Spectra in Alpha Quartz. *Phys. Rev. B* **1970**, *1*, 4179.
(13) Totzeck, M. Numerical Simulation of High-NA Quantitative Polarization Microscopy and Corresponding Near-Fields. *Optik* **2001**, *112*, 399−406.
(14) Caballero, M. T.; Ibanez-Lopez, C.; Martinez-Corral, M. Shaded-Mask Filtering: Novel Strategy for Improvement of Resolution in Radial-Polarization Scanning Microscopy. *Opt. Eng.* **2006**, *45*, 098003.
(15) Iglesias, I.; Vohnsen, B. Polarization Structuring for Focal Volume Shaping in High-Resolution Microscopy. *Opt. Commun.* **2007**, *271*, 40−47.
(16) Chen, W. B.; Zhan, Q. W. Creating a Spherical Focal Spot with Spatially Modulated Radial Polarization in 4π Microscopy. *Opt. Lett.* **2009**, *34*, 2444−2446.
(17) Sheppard, C. J. R.; Gong, W.; Si, K. Polarization Effects in 4π Microscopy. *Micron* **2011**, *42*, 353−359.
(18) Weiner, M. Ultrafast Optical Pulse Shaping: A Tutorial Review. *Opt. Commun.* **2011**, *284*, 3669−3692.
(19) Beresna, M.; Gecevicius, M.; Kazansky, P. G.; Gertus, T. Radially Polarized Optical Vortex Converter Created by Femtosecond Laser Nanostructuring of Glass. *Appl. Phys. Lett.* **2011**, *98*, 201101.
(20) Guo, D.; Sakamoto, K.; Miki, K.; Ikeda, S.; Saiki, K. Alignment-Induced Epitaxial Transition in Organic−Organic Heteroepitaxy. *Phys. Rev. Lett.* **2008**, *101*, 3−6.
(21) *Applied Scanning Probe Methods*; Bhushan, B., Fuchs, H., Kawata, S., Eds.; Springer-Verlag: Heidelberg, Germany, 2007; Vol. *6*.
(22) Kneipp, K.; Wang, Y.; Kneipp, H.; Perelman, L. T.; Itzkanm, I.; Dasari, R. Single Molecule Detection Using Surface-Enhanced Raman Scattering (SERS). *Phys. Rev. Lett.* **1997**, *78*, 1667−1670.
(23) Hayazawa, N.; Inouye, Y.; Sekkat, Z.; Inouye, Y.; Kawata, S. Metallized Tip Amplification of Near-Field Raman Scattering. *Opt. Commun.* **2000**, *183*, 333−336.
(24) Stöckle, R. M.; Suh, Y. D.; Deckert, V.; Zenobi, R. Nanoscale Chemical Analysis by Tip-Enhanced Raman Spectroscopy. *Chem. Phys. Lett.* **2000**, *318*, 131−136.
(25) Hayazawa, N.; Saito, Y.; Kawata, S. Detection and Characterization of Longitudinal Field for Tip-Enhanced Raman Spectroscopy. *Appl. Phys. Lett.* **2004**, *85*, 6239−6241.
(26) Saito, Y.; Hayazawa, N.; Kataura, H.; Murakami, T.; Tsukagoshi, K.; Inouye, Y.; Kawata, S. Polarization Measurements in Tip-Enhanced Raman Spectroscopy Applied to Single-Walled Carbon Nanotubes. *Chem. Phys. Lett.* **2005**, *410*, 136−141.
(27) Jorio, A.; Pimenta, M. A.; Filho, A. G.; Samsonidze, G. G.; Swan, A. K.; Ünlü, M. S.; Goldberg, B. B.; Saito, R.; Dresselhaus, G.; Dresselhaus, M. S. Resonance Raman Spectra of Carbon Nanotubes by Cross-Polarized Light. *Phys. Rev. Lett.* **2003**, *90*, 107403.
(28) Saito, Y.; Ohashi, Y.; Verma, P. Optimization of *S*-Polarization Sensitivity in Apertureless near-Field Optical Microscopy. *Int. J. Optics* **2012**, *2012*, 962317.
(29) Sanchez, E. J.; Novotny, L.; Xie, X. S. Near-Field Fluorescence Microscopy Based on Two-Photon Excitation with Metal Tip. *Phys. Rev. Lett.* **1999**, *82*, 4014−4017.
(30) Saito, Y.; Murakami, T.; Inouye, Y.; Kawata, S. Fabrication of Silver Probes for Localized Plasmon Excitation in Near-Field Raman Spectroscopy. *Chem. Lett.* **2005**, *34*, 920−921.
(31) Merlen, A.; Valmalette, J. C.; Gucciardi, P. G.; de la Chapelle, M. L.; Frigoute, A.; Ossikovskie, R. Depolarization Effects in Tip-Enhanced Raman Spectroscopy. *J. Raman Spectrosc.* **2009**, *40*, 1361−1370.
(32) Hermann, P.; Hecker, M.; Chumakov, D.; Weisheit, M.; Rinderknecht, J.; Shelaev, A.; Dorozhkin, P.; Eng, L. M. Imaging and Strain Analysis of Nano-Scale SiGe Structures by Tip-Enhanced Raman Spectroscopy. *Ultramicroscopy* **2011**, *111*, 1630−1635.
(33) Schnell, M.; Garcia-Etxarri, A.; Alkorta, J.; Aizpurua, J.; Hillenbrand, R. Phase-Resolved Mapping of the Near-Field Vector and Polarization State in Nanoscale Antenna Gaps. *Nano Lett.* **2010**, *10*, 3524−3528.
(34) Berweger, S.; Raschke, M. B. Polar Phonon Mode Selection Rules in Tip-Enhanced Raman Scattering. *J. Raman Spectrosc.* **2009**, *40*, 1413−1419.
(35) Konishi, K.; Nomura, M.; Kumagai, N.; Iwamoto, S.; Arakawa, Y.; Gonokami, M. Circularly Polarized Light Emission from Semiconductor Planar Chiral Nanostructures. *Phys. Rev. Lett.* **2011**, *106*, 057402.
(36) Toleutaev, B. N.; Tahara, T.; Hamaguchi, H. Broadband Multiplex CARS Spectroscopy Application to Polarization Sensitive and Time Resolved Measurements. *Appl. Phys.* **1994**, *B59*, 369−375.
(37) Okuno, M.; Kano, H.; Leproux, P.; Couderc, V.; Hamaguchi, H. Ultrabroadband Multiplex CARS Microspectroscopy and Imaging using a Subnanosecond Supercontinuum Light Source in the Deep Near Infrared. *Opt. Lett.* **2008**, *33*, 923−925.
(38) Freudiger, C. W.; Min, W; Holtom, G. R.; Xu, B. W.; Dantus, M; Xie, X. S. Highly Specific Label-Free Molecular Imaging with Spectrally Tailored Excitation-Stimulated Raman Scattering (STE-SRS) Microscopy. *Nat. Photonics* **2011**, *5*, 103−109.
(39) Lu, F.; Zheng, W.; Sheppard, C.; Huang, Z. Interferometric Polarization Coherent Anti-Stokes Raman Scattering (IP-CARS) Microscopy. *Opt. Lett.* **2008**, *33*, 602−604.
(40) Orsel, K.; Garbacik, E. T.; Jurna, M.; Korterik, J. P.; Otto, C.; Herek, J. L.; Offerhaus, H. L. Heterodyne Interferometric Polarization Coherent Anti-Stokes Raman Scattering (HIP-CARS) spectroscopy. *J. Raman. Spectrosc.* **2010**, *41*, 1678−1681.
(41) Freudiger, C. W.; Roeffaers, M. B. J.; Zhang, X.; Saar, B. G.; Min, W.; Xie, X. S. Optical Heterodyne-Detected Raman-Induced Kerr Effect (OHD-RIKE) Microscopy. *J. Phys. Chem. B.* **2011**, *115*, 5574−5581.